Decentralized Control of DC Electric Springs for Storage Reduction in DC Microgrids

Ming-Hao Wang, *Member, IEEE*, Shuo Yan, *Member, IEEE*, Siew-Chong Tan, *Senior Member, IEEE*, Zhao Xu, *Senior Member, IEEE*, and Shu Yuen Hui, *Fellow, IEEE*

***Abstract*—Series dc electric springs (series ESs) can tackle the intermittency of the renewable generations (RGs) with reduced storage capacity in dc microgrids (MGs). They can actively manipulate the power profiles of the serially connected noncritical loads (NCLs) to follow the fluctuating RG. In the process of regulating the dc bus voltages, the power rating of an NCL can affect the power of its corresponding series ES. If multiple series ESs with differently rated NCLs can be operated in a coordinative way, the total storage capacity of the series ESs can be potentially reduced. In this article, a decentralized controller is proposed to coordinate the operations of multiple series ESs such that the required storage capacity of the series ESs can be reduced. The conditions for achieving the minimum battery charging and discharging power are analytically derived. The stability analysis of the system as well as the design of the decentralized controller is provided. Experiment results on a 120-V dc grid confirmed that the proposed controller can effectively reduce the total storage capacity of the series ESs in dc MGs by 7.5%.**

***Index Terms*—Battery energy storage, dc microgrids (MGs), electric springs, power electronics, smart load, stability.**

I. Introduction

DC GRIDS have been widely applied for their high efficiency and simple incorporation of the renewable generations (RGs) [1]. To provide stable power supplies for the critical loads (CLs) [2], battery energy storages are typically adopted to buffer the fluctuations caused by the intermittency of the RGs [3]. However, considering the potential environmental damage and high cost of batteries [4], the capacity of the batteries should be minimized.

Among the existing solutions of balancing the supply and demand in power grids [5]–[11], the use of smart loads can be a cost-effective solution in reducing energy storage capacity, particularly in view of the growing penetration of intermittent RGs. The series ES is a possible means of implementing the smart load. As reported in [12] and [13], the dc electric springs can do the following:

1) provide real-time demand side management for eliminating the bus voltage variation [14];
2) perform active power filtering for buffering the harmonic power [10];
3) eliminate the voltage droop along the distribution lines; and
4) provide fault-ride-through support for the CLs in dc power systems.

They can be typically applied in data center, telecommunication system, LED-based lighting system, and traction system. The series ES is essentially a controllable bipolar voltage source, which is connected in series with a noncritical load (NCL) to form a smart load. It is capable of real-time bus voltage regulation and automatic NCL power adjustment. The series ES can effectively reduce the required battery storage capacity of a dc grid via the active load control of the NCL [13]. When the series ESs are connected to different power-rated NCLs, the charging and discharging powers of their battery storages will be different. In view of this, the required storage capacity of a dc grid can be further reduced if multiple series ESs can be operated in a cooperative way. To achieve this, a coordinative control scheme will be needed for the series ESs.

Control methods for coordinating multiple converters can be generally categorized into centralized control [15]–[17], distributed control [18]–[20], and decentralized control [21]–[23]. Although the centralized control scheme can achieve accurate power control of the overall grid for long-term operations (e.g., in hours) [15], [16], [24], it cannot cope with the fast time-variant RGs in a real-time manner due to the limitation of the communication bandwidth [25]. For the distributed control scheme, it can have a less sophisticated communication network than that of the centralized control method [18]. Mathematically, by formulating the optimization problem (e.g., minimization of generation cost [26]) of the power grid and solving its equilibrium problem in a distributed way, the operating points of power grid will ultimately converge to the global optimum. However, this control scheme demands convexity of the original problem and its design procedure is relatively complicated. Furthermore, the propagation delay of the connected network for the distributed control scheme will confine the speed of convergence, which makes it incapable of dealing with fast power variations

Manuscript received April 9, 2019; revised June 21, 2019 and August 28, 2019; accepted September 14, 2019. Date of publication September 19, 2019; date of current version February 11, 2020. This work was supported by the Hong Kong Research Grant Council under the Theme-based Project T23-407/13N and Project T23-701/14-N. This article was presented in part at the IEEE Energy Conversion Congress and Exposition, Milwaukee, WI, USA, September 2016. Recommended for publication by Associate Editor F. W. Fuchs. *(Corresponding author: Ming-Hao Wang.)*

M.-H. Wang and Z. Xu are with the Department of Electrical Engineering, The Hong Kong Polytechnic University, Hong Kong (e-mail: minghaow@connect.hku.hk; zhao.xu@polyu.edu.hk).

S. Yan, S.-C. Tan, and S. Y. Hui are with the Department of Electrical and Electronic Engineering, The University of Hong Kong, Hong Kong (e-mail: shuo.yan@rmit.edu.au; sctan@eee.hku.hk; ronhui@eee.hku.hk).

Color versions of one or more of the figures in this article are available online at http://ieeexplore.ieee.org.

Digital Object Identifier 10.1109/TPEL.2019.2942604

of dc microgrids (MGs). The decentralized control method, e.g., droop control [21], [22], does not require communication networks. Since it only requires the local information for the derivation of control signals, it has low computation complexity and can achieve a fast dynamic response of the system. Although the tight regulation of the mains voltage is generally sacrificed for achieving the cooperative operation of multiple converters, the deviation of the mains voltage can still be maintained within the acceptable range of the most appliances. By comparison, the decentralized control methods are relatively more viable for coordinating multiple series ESs in pacifying the fast time-variant power of the RGs in dc MGs.

Among the reported research work on decentralized control of dc MGs, the research focuses are mainly on the responsibility sharing of multiple dc appliances. In [27], a mode-adaptive droop control is reported for coordinating the operations of RGs, storages, and utility grid interfaced converter in dc MGs. As the economic operation of dc MGs is becoming increasingly important, the recent researches are trying to incorporate the economic objective into the design of the decentralized controller. In [23] and [28], the battery state of charge (SoC) is used to determine the droop coefficient for SoC equalization of multiple storage systems. To further improve the accuracy of responsibility sharing among interfaced converters, a low-bandwidth communication-based droop control is reported in [29]. In [30], a decentralized economic power sharing control is proposed for minimizing the generation cost of multiple distributed generators (DGs) in dc MGs. As the incremental costs of DGs are linearly associated with the dc bus voltage, it can be conveniently mapped into the droop curve of the DGs without adding an extra communication network. However, as the power of series ES is nonlinearly changed with respect to the power fluctuation of MGs [12], [13], the conventional decentralized control is no more feasible and the recent researches on ES [19], [20] tend to use a communication-based control scheme for achieving better coordination. To regulate the bus voltage against the volatile RG, a new decentralized control scheme is proposed in this article. This control scheme can coordinate the operation of multiple series ESs for achieving a reduced storage capacity. It is worth mentioning that the proposed control scheme is different from the conventional droop control in many ways. It has a faster dynamic response than that of the conventional centralized and distributed control methods due to the omission of communication systems. In addition, different from the conventional droop control schemes, the proposed controller is programmed with the objective of reducing the net storage capacity of series ESs for the first time. The nonlinear power curve of multiple series ES is mathematically analyzed. Based on this, the proposed controller is designed for minimizing the total charging and discharging power of the series ESs when regulating the bus voltage. The state-space model of the dc MG with the constant power load and multiple series ESs is derived for the stability analysis. A simulation is performed to demonstrate the stability improvement of the dc MG with the series ESs. Experiments on a 120-V dc MG have been conducted to validate the storage reduction functionality of the proposed control scheme.

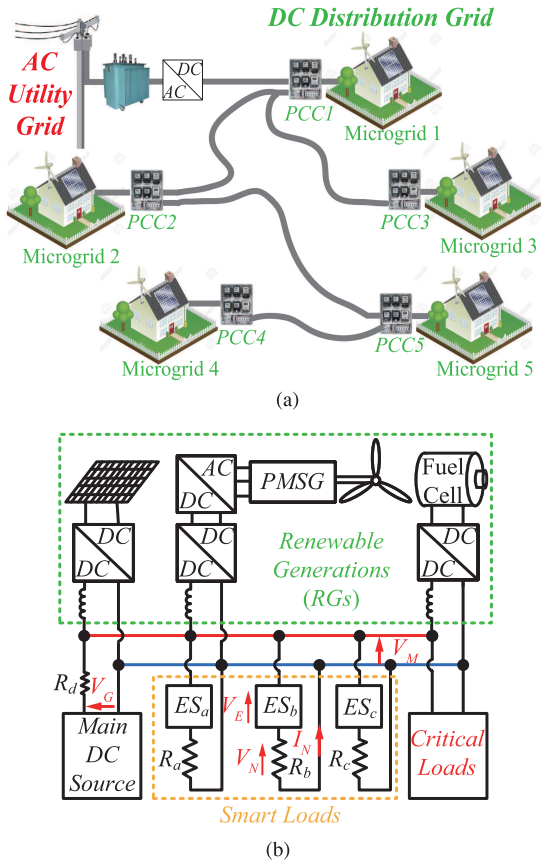

Fig. 1. Illustrations of (a) dc distribution grid and (b) dc MG with multiple series ESs.

II. DC MG With Multiple Series DC Electric Springs

Fig. 1(a) illustrates the emerging dc distribution grids. The dc MGs, which are clusters of low-peripheral low-voltage appliances, are essentially the subnetworks of the dc distribution grid. They are interconnected through the distribution lines and form different points of common coupling (PCC) in the dc distribution grid. Fig. 1(b) shows the circuit diagram of a dc MG with multiple series ESs installed at PCC. The main dc power source V_G and distribution lines R_d are essentially the Thevenin equivalent circuit of the dc distribution grid. The main dc source delivers a stable base power of P_G to the MG. The RGs (e.g., PV panel, wind generation, and fuel cell) inject intermittent power P_R into the dc bus. This will lead to a fluctuating PCC voltage V_M. R_a, R_b, and R_c are the NCLs (e.g., electric water heaters) with different nominal powers of P_a, P_b, and P_c ($P_a < P_b < P_c$). They can tolerate a certain degree of fluctuations on their supply voltages V_N. The CLs are normally electronic loads, which cannot tolerate large fluctuations on the supply voltage V_M. The series ES is a distributed onsite voltage regulation technology. Each series ES is connected to an NCL to form a smart load. The series can be achieved by a full-bridge converter with dc-link battery storages. It imposes a tuning voltage V_E to adjust the NCL current I_N. As reported in [12], the NCL can be the following:

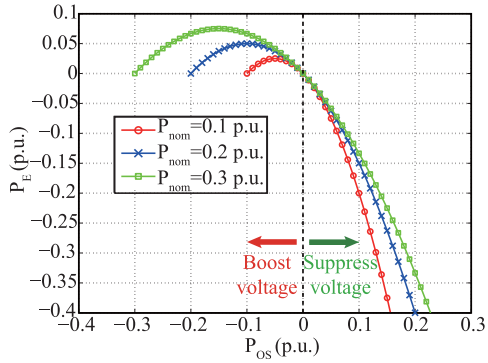

Fig. 2. P_E curves with different power-rated NCLs.

1) positive constant-resistive loads;
2) negative constant-resistive loads;
3) positive constant-power loads (CPLs);
4) negative CPLs.

Since most of the NCLs are dissipative thermoelectric loads [8], [12], [13], [31], the NCL is considered as a resistor R_N in this article. Thus, it can be derived that

$$\begin{cases} P_{\text{nom}} = \dfrac{V_M^2}{R_N} \\ P_{\text{SL}} = \dfrac{V_M(V_M - V_E)}{R_N} \\ P_E = \dfrac{V_E(V_M - V_E)}{R_N} \end{cases} \tag{1}$$

where P_{nom}, P_{SL}, and P_E are the nominal power of NCL, smart load power, and power of series ES, respectively. The profiles of P_{SL} can be controlled to follow the generation profiles of the RGs so that a stable power supply of the CLs can be obtained. In the meantime, the power quality of the NCL is compromised.

III. Operating Curves of Series ESs

By neglecting the power loss on the distribution cable, the fluctuating part of the grid power P_{OS} can be expressed as

$$P_{\text{OS}} = P_G + P_R - P_{\text{CL}} - P_{\text{nom}} \tag{2}$$

where P_{CL} is the nominal power of CL. When a smart load is operated to compensate P_{OS}, the power change in the smart load will be equal to P_{OS}, i.e.,

$$P_{\text{OS}} = P_{\text{SL}} - P_{\text{nom}}. \tag{3}$$

P_E can be expressed as follows by combining (1) and (3):

$$P_E = (P_{\text{OS}} + P_{\text{nom}}) - \frac{(P_{\text{OS}} + P_{\text{nom}})^2}{P_{\text{nom}}}. \tag{4}$$

By normalizing (4) in a per-unit (p.u.) system with the base of the system rated power P_S, the profiles of P_E can be plotted with respect to the variation of P_{OS} as shown in Fig. 2. Here, P_{nom} is set to be 0.1 p.u., 0.2 p.u., and 0.3 p.u. to represent a light load, a medium load, and a heavy load, respectively. V_E cannot exceed V_M to inverse the polarity of V_N. As shown in Fig. 2, the series ES with the light load has the minimum charging power when these series ESs are operated to boost V_M against negative P_{OS}. The series ES with the heavy load has the maximum discharging power when these series ESs are operated to suppress V_M against positive P_{OS}. By engaging different smart loads in compensating P_{OS}, the required power of these series ESs will be different. This offers potential of reducing the required storage capacity.

IV. Derivations of the Minimum Charging and Discharging Power

When three series ESs are operated to regulate V_M, P_{OS} is jointly compensated by the smart loads and each one compensates the corresponding proportion of a, b, and c. According to (4), the power of a series ES can be expressed as follows:

$$P_{E\_x} = (xP_{\text{OS}} + P_x) - \frac{(xP_{\text{OS}} + P_x)^2}{P_x} \ \forall x = \{a, b, c\} \tag{5}$$

where

$$\begin{cases} a + b + c = 1 \\ 0 \le a, b, c \le 1. \end{cases} \tag{6}$$

In (5), P_{E_x} denotes the power of ES$_x$. P_x is the nominal power of the NCL x. By rearranging (5), the total power of the series ESs can be written as follows:

$$\begin{cases} P_T = \sum_{x=\{a,b,c\}} P_{E\_x} = -P_{\text{OS}} - P_{\text{OS}}^2\sigma \\ \sigma = \sum_{x=\{a,b,c\}} x^2 P_x^{-1}. \end{cases} \tag{7}$$

As shown in (7), σ will affect the value of P_T. Mathematically, the upper and lower bounds of σ can be derived according to the inequalities of arithmetic and geometric means, i.e.,

$$\begin{cases} \text{LB} \le \sigma \le \text{UB} \\ \text{LB} = \dfrac{(a+b+c)^2}{P_a + P_b + P_c} \\ \text{UB} = \left(\dfrac{a}{\sqrt{P_a}} + \dfrac{b}{\sqrt{P_b}} + \dfrac{c}{\sqrt{P_c}}\right)^2. \end{cases} \tag{8}$$

By (7), the total accumulated energy of the ESs can be expressed as follows:

$$E_T(t) = \int_0^t P_T(t)dt = \int_0^t [-P_{\text{OS}}(t) - P_{\text{OS}}^2(t)\sigma(t)]dt. \tag{9}$$

The minimum required storage capacity of the series ESs should be at least greater than the maximum deviation of $E_T(t)$, i.e.,

$$\begin{aligned} C_{\min} = &\max\left(\int_0^t [-P_{\text{OS}}(t) - P_{\text{OS}}^2(t)\sigma(t)]dt\right) \\ &- \min\left(\int_0^t [-P_{\text{OS}}(t) - P_{\text{OS}}^2(t)\sigma(t)]dt\right) \end{aligned} \tag{10}$$

Therefore, in the voltage boosting operations ($P_{\text{OS}} < 0$ and $P_T > 0$), a large σ is preferred so that the charging power of batteries can be small. In the voltage suppression operations ($P_{\text{OS}} > 0$ and $P_T < 0$), a small σ is preferred so that a small discharging power of batteries can be achieved. Correspondingly,

the criterion of achieving the maximum and minimum values of σ can be expressed as follows:

$$\sigma = \begin{cases} \text{LB} & \text{when } \dfrac{a}{P_a} = \dfrac{b}{P_b} = \dfrac{c}{P_c} \\ \text{UB} & \text{when } \sum_{x,y=a,b,c\, x\neq y} xy = 0. \end{cases} \tag{11}$$

By (11), the minimum charging power of P_T can be achieved by operating a single smart load to boost V_M. However, this operation cannot always be achieved since the allowable voltage deviation of an NCL is limited. Considering that the ES voltages are limited within a range of

$$V_{\min} \le V_x \le V_{\max} \quad \forall x = \{a, b, c\} \tag{12}$$

where V_x is the output voltage of ES_x. A suboptimal compensation strategy for voltage boosting operations can be derived to achieve a small charging power of the series ESs. Specifically, when $P_{\text{OS}} < 0$, W and V_M fall below the reference, ES_a with the light NCL (P_a) will be first activated to boost V_M. In the meantime, ES_b and ES_c, which are connected with larger power-rated NCLs, fix their voltage outputs at 0 V. When V_a reaches $V_{\max}$ and V_M decreases, ES_b with the medium NCL (P_b) will be activated. In the meantime, V_a is controlled to be $V_{\max}$ and ES_c stays unactivated. When V_M is kept falling and V_b reaches $V_{\max}$, ES_a and ES_b are controlled to deliver the maximum voltages. ES_c starts to shed the NCL by following the same analogy until all series ESs eventually reach their respective output limits.

According to (11), for the voltage suppression operation, the minimum discharging power of the series ESs can be achieved by satisfying

$$\frac{aP_{\text{OS}}}{P_a} = \frac{bP_{\text{OS}}}{P_b} = \frac{cP_{\text{OS}}}{P_c}. \tag{13}$$

Since xP_{OS} will be compensated by the smart load x, it can be derived that

$$xP_{\text{OS}} = \frac{V_M(V_M - V_x)}{R_x} - \frac{V_M^2}{R_x} = -\frac{V_M V_x}{R_x} \quad \forall x = \{a, b, c\}. \tag{14}$$

By substituting (14) into (13), it can be derived that

$$\frac{xP_{\text{OS}}}{P_x} = \frac{-V_M V_x}{P_x R_x} = \frac{-V_M V_x R_x}{R_x V_M^2} = \frac{-V_x}{V_M} \quad \forall x = \{a, b, c\}. \tag{15}$$

According to (13) and (15), the condition for achieving the minimum discharging power in voltage suppression operations can be expressed as

$$V_a = V_b = V_c. \tag{16}$$

When the operating voltages of series ESs are determined, the rated powers of the series ESs' dc-link storages can be confirmed. By (1), it can be derived that

$$\frac{P_E}{P_{\text{nom}}} = \frac{V_E(V_M - V_E)}{V_M^2}. \tag{17}$$

As illustrated in Fig. 2 and (1), the ES powers in voltage suppression operations ($V_E < 0$) are larger than the cases of voltage boosting operations ($V_E > 0$). Since the voltages of the series ESs are identical during the voltage suppression operations, the rated power of dc-link storages should fulfill

$$P_{\text{rate}} \ge P_{\text{nom}} \frac{V_{\min}(V_M - V_{\min})}{V_M^2} \tag{18}$$

and the power ratings of the storages can be determined for the respective series ESs by using (18).

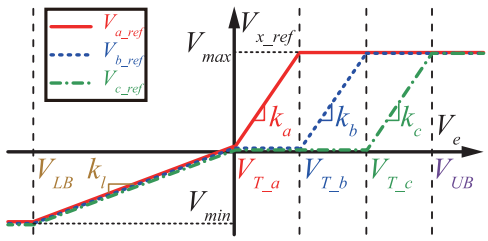

Fig. 3. Voltage droop curves of the series ESs. (V_{T_x} are the voltage thresholds of ES_x. k_x and k_l are the droop coefficients. $x = \{a, b, c\}$).

V. Design of the Decentralized Controller

A. Voltage Droop Controller

Based on the analyses given in Section IV, a desirable compensation strategy for achieving the minimum charging and discharging power can be summarized. When multiple series ESs, which are connected with differently rated NCLs, are operated to boost the PCC voltage, the series ESs should be activated from the ES with the minimally rated NCL to the ES with the maximally rated NCL. When the voltage of a series ES reaches the maximum and the bus voltage is falling, the series ES with the next larger power-rated NCL will be activated. By following this analogy, the series ESs are sequentially activated until all series ESs reach their respective maximum output voltages. For voltage suppression operations, the output voltages of the series ESs should be controlled to be identical. Based on this principle, the droop curves of ES voltage references V_{ref_x} can be plotted as shown in Fig. 3.

As shown in Fig. 3, the voltage error V_e between the bus voltage reference V_{M_ref} and the measured bus voltage V_M is used to determine the voltage references of the respective series ES. V_e has been divided into six bands and the series ESs will be controlled differently in each band. When V_M sags and V_e exceeds the voltage threshold of V_{T_a}, V_{a_ref} will be increased to operate ES_a in voltage boosting operation until it reaches $V_{\max}$. In the meantime, V_{b_ref} and V_{c_ref} are set at 0 V. When V_e exceeds the voltage threshold of V_{T_b}, V_{b_ref} rises to shed R_b until it reaches $V_{\max}$. Meanwhile, $V_{a\_\text{ref}} = V_{\max}$ and $V_{c\_\text{ref}} = 0$ V. When V_e exceeds the threshold of V_{T_c}, $V_{a\_\text{ref}} = V_{b\_\text{ref}} = V_{\max}$ and V_{c_ref} will be increased linearly to engage ES_c in load shedding. When $V_e > V_{\text{UB}}$, all referenced voltages of the series ESs will be set to the maximum.

When V_M surges and $V_e < 0$, the voltage references of series ESs will be set at the same values. When V_e reaches the lower bound of V_{LB}, the series ES voltages will be controlled at $V_{\min}$. Mathematically, the ES voltage references described in Fig. 3

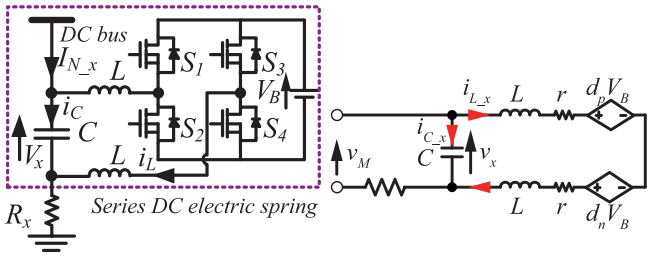

Fig. 4. Circuit diagrams of (a) smart load x and (b) equivalent circuit of smart load x. ($x = \{a, b, c\}$).

can be expressed as

$$\forall x = \{a, b, c\}$$

$$V_{\text{ref\_}x} = \begin{cases} V_{\max}, & V_e \geq \left(V_{T\_x} + \dfrac{V_{\max}}{k_x}\right) \quad (19a) \\ k_x(V_e - V_{T\_x}), & V_{T\_x} < V_e < \left(V_{T\_x} + \dfrac{V_{\max}}{k_x}\right) \quad (19b) \\ 0, & 0 \leq V_e \leq V_{T\_x} \quad (19c) \\ k_l V_e, & \dfrac{V_{\min}}{k_l} \leq V_e < 0 \quad (19d) \\ V_{\min}, & V_e < \dfrac{V_{\min}}{k_l} \quad (19d) \end{cases}$$

where V_{T_x} are the voltage thresholds of ES$_x$. k_x and k_l are the droop coefficients.

B. Voltage Controller of Series ESs

The circuit diagram of smart load x is shown in Fig. 4(a). Two in-phase sawtooth carriers are used for the modulation of the two bridge branches. By averaging the smart load branch over one switching period, the equivalent circuit diagram of smart load x can be plotted as shown in Fig. 4(b), where r is the equivalent series resistor of inductor L. The duty ratios of S_1 and S_3 are defined as d_p and d_n, respectively.

According to Fig. 4(b), the state-space model of the smart load can be expressed as

$$\begin{bmatrix} \dot{v}_x \\ \dot{i}_{L\_x} \end{bmatrix} = \begin{bmatrix} -\dfrac{1}{R_x C} & -\dfrac{1}{C} \\ \dfrac{1}{2L} & -\dfrac{r}{L} \end{bmatrix} \begin{bmatrix} v_x \\ i_{L\_x} \end{bmatrix} + \begin{bmatrix} \dfrac{V_M}{R_x C} \\ -\dfrac{\Delta d V_B}{2L} \end{bmatrix} \quad (20)$$

where $\Delta d = d_p - d_n$. According to (20), the voltage–current cascaded control block diagram of a series ES can be plotted as shown in Fig. 5, where G_V and G_I are the transfer functions of the capacitor voltage controller and the inductor current controller. Their control parameters can be obtained by using the loop-shaping method.

To ensure the stability of the system, it is desirable to set the crossover frequency f_{ci} of the current loop to one-tenth of the switching frequency f_s [32]. Thus, the closed-loop transfer

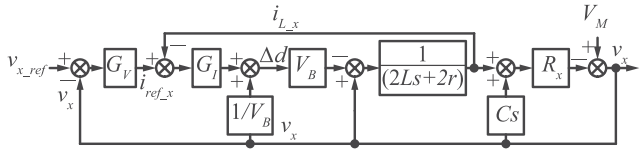

Fig. 5. Voltage–current cascaded control block diagram of ES$_x$ ($x = \{a, b, c\}$).

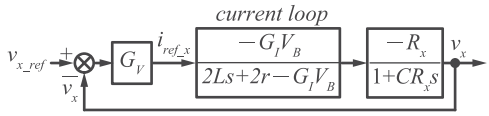

Fig. 6. Simplified control block diagram of ES$_x$ ($x = \{a, b, c\}$).

function of the current loop can be expressed as

$$H_{ci} = \frac{-G_I V_B}{2Ls + 2r - G_I V_B} = \frac{0.2\pi f_s}{0.2\pi f_s + s}. \quad (21)$$

Therefore, G_I can be derived as

$$G_I = -\frac{0.4(Ls + r)\pi f_s}{V_B s} = -\frac{0.4L\pi f_s}{V_B} - \frac{0.4r\pi f_s}{V_B}\frac{1}{s}. \quad (22)$$

By closing the inner current loop shown in Fig. 5, a simplified control block diagram of the series ES can be plotted as shown in Fig. 6.

In Fig. 6, G_V is essentially a lead–lag compensator, which has a transfer function of

$$G_V = -\frac{A_x(1 + sT_n)}{1 + sT_d} \quad \forall x = \{a, b, c\} \quad (23)$$

where A_x is the proportional gain. T_n and T_d are the time constants. By setting $T_n = CR_x$, the closed-loop transfer function of the system shown in Fig. 6 can be expressed as

$$\begin{aligned} H_{\text{cl\_}x} &= \frac{0.2\pi f_s A_x R_x}{(0.2\pi f_s + s)(1 + sT_d) + 0.2\pi f_s A_x R_x} \\ &= \frac{0.2\pi f_s A_x R_x}{T_d s^2 + (1 + 0.2\pi f_s T_d)s + 0.2\pi f_s (1 + A_x R_x)} \end{aligned} \quad (24)$$

where $H_{\text{cl\_}x}$ is a typical second-order system. The damping ratio ξ and natural frequency ω_n of $H_{\text{cl\_}x}$ can be expressed as

$$\begin{cases} \omega_n = \sqrt{\dfrac{0.2\pi f_s (1 + A_x R_x)}{T_d}} \\ \xi = \dfrac{1 + 0.2\pi f_s T_d}{2\omega_n T_d} \\ T_s = \dfrac{4}{\xi \omega_n} \end{cases} \quad (25)$$

where T_s is the settling time with 2% steady-state error. Empirically, in order to obtain a fast and damped dynamic response of a system, it is desirable to set $\xi = 0.707$ [33]. Here, T_s is set to be 0.65 ms so that the series ESs can have a similar dynamic response. As a result, A_x and T_d can be derived accordingly. Table I shows the specifications of the ES and the DC MG.

TABLE I
SPECIFICATIONS OF THE SERIES ES AND DC MG

Description	Parameter	Value
Referenced bus voltage	V_{M_ref}	120 V
Filter capacitance	C	15 μF
Filter inductor	L	3.3 mH
Batteries	V_B	5×12 V (five cells)
Switching frequency	f_s	20 kHz
DSP controller		TMS320F28069
Main dc source	V_G	117.5 V
Distribution resistance	R_d	1.6 Ω
DC-link capacitance	C_{DC}	1000 μF
RG	P_R	$0 \sim 2216$ W
CL	P_{CL}	400 W
NCL	R_a	144 Ω
	R_b	72 Ω
	R_c	48 Ω

TABLE II
PARAMETERS OF VOLTAGE–CURRENT CASCADED CONTROLLERS

Description	Parameter	Value
Current controller	G_I	$-1.38-125.67s^{-1}$
Voltage controller of ES_a	G_V	$(-2.941s-1362)/(31.2s+1)$
Voltage controller of ES_b		$(-2.941s-2723)/(31.2s+1)$
Voltage controller of ES_b		$(-2.941s-4085)/(31.2s+1)$

Based on the specifications shown in Table I, the control parameters of the voltage–current cascaded controllers can be summarized as shown in Table II. By adopting the control parameters shown in Table II, the closed-loop transfer functions of the smart loads will be identical, i.e.,

$$H_{cl} = H_{\text{cl\_}a} = H_{\text{cl\_}b} = H_{\text{cl\_}c}. \tag{26}$$

VI. STABILITY ANALYSIS

A. State-Space Model of Series ES Integrated DC MG

It is reported in [34] that the nonlinear behavior of the maximum power point tracking (MPPT) control, e.g., perturb and observation control, can affect the stability of the grid. For conducting a simplified analysis, the dynamics of the MPPT control are neglected in this article and the RG is modeled as a constant power source (CPS). For the CL, it is considered as a CPL [35]. Since the input voltage of the CPL and the output voltage of the CPS are clamped to the dc bus voltage, it can be derived that

$$i = \frac{P}{v_M} \quad \forall i = \{i_R, i_{\text{CL}}\}, P = \{P_R, P_{\text{CL}}\} \tag{27}$$

where i_R and i_{CL} are the currents of the CPS and CPL, respectively. By linearizing (27) at the point of $(\frac{P}{V_M}, V_M)$, i.e.,

$$\begin{aligned} \frac{v_M - V_M}{i - \dfrac{P}{V_M}} &= \frac{dv_M}{di} \\ \frac{v_M - V_M}{i - \dfrac{P}{V_M}} &= -\frac{{V_M}^2}{P} \end{aligned} \tag{28}$$

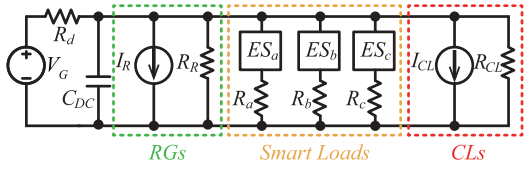

Fig. 7. Simplified circuit diagram of the dc MG shown in Fig. 1(b).

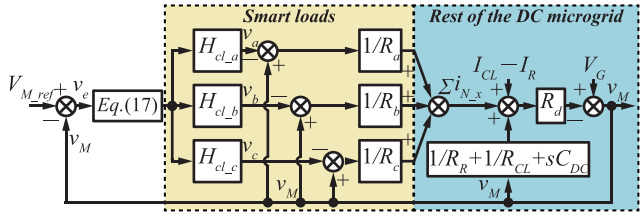

Fig. 8. Overall decentralized control block diagram of the dc MG.

the small-signal models of CPS and CPL can be obtained as follows:

$$i = -\frac{P}{{V_M}^2} v_M + \frac{2P}{V_M} \quad \forall i = \{i_R, i_{\text{CL}}\}, P = \{P_R, P_{\text{CL}}\}. \tag{29}$$

According to (29), the CPS and CPL can be equivalent as a current source of $2\frac{P}{V_M}$ in parallel with a resistance of $-\frac{{V_M}^2}{P}$ [35], [36], i.e.,

$$\begin{cases} R_R = -\dfrac{V_M^2}{P_R}, & I_R = 2\dfrac{P_R}{V_M} \\ R_{\text{CL}} = -\dfrac{V_M^2}{P_{\text{CL}}}, & I_{\text{CL}} = 2\dfrac{P_{\text{CL}}}{V_M}. \end{cases} \tag{30}$$

Therefore, the simplified circuit diagram of the dc MG can be plotted as shown in Fig. 7.

The overall decentralized voltage control block diagram of the dc MG can be derived as shown in Fig. 8. The design of the control parameters is based on the specifications listed in Table I. The voltage error v_e will be fed to a voltage droop controller to generate the voltage references $V_{\text{ref\_}x}$ of each series ES. The output voltages of the series ESs are controlled to track $V_{\text{ref\_}x}$, where the subscript $x = a, b$, or c.

With the closed-loop control, the dynamics of ES_x can be expressed as

$$\begin{cases} \dfrac{dv_x}{dt} = \dfrac{v_M}{CR_x} - \dfrac{v_x}{CR_x} - \dfrac{i_{L\_x}}{C} \\ i_{L\_x} = i_{\text{ref\_}x} H_{ci} \\ i_{\text{ref\_}x} = (V_{\text{ref\_}x} - v_x) G_{V\_x}. \end{cases} \tag{31}$$

Based on the linearized small-signal circuit model shown in Fig. 7, the dynamics of the series ESs integrated dc MG can be expressed by

$$\begin{aligned} \frac{V_G - v_M}{R_d} = C_{\text{DC}} \frac{dv_M}{dt} + \sum_{x=\{a,b,c\}} \frac{v_M - v_x}{R_x} \\ + \frac{v_M}{R_{\text{CL}}} + \frac{v_M}{R_R} + I_{\text{CL}} + I_R. \end{aligned} \tag{32}$$

By combining (19), (31), and (32), the overall state-space model of the dc MG can be derived as

$$\dot{X} = A \cdot X + C \tag{33}$$

where $X = [v_M, v_a, i_{\text{ref\_}a}, i_{L\_a}, v_b, i_{\text{ref\_}b}, i_{L\_b}, v_c, i_{\text{ref\_}c}, i_{L\_c}]^T$. Since the droop coefficient of ES_x will be changed according to the steady-state operating point, the state-space model will also be changed accordingly. In the voltage suppression operation, i.e., when $\frac{V_{\min}}{k_l} \le V_e < 0$ (34) shown at the bottom of this page, and

$$\begin{aligned} C = \Bigg[& \frac{V_G}{R_d C_{\text{DC}}} - \frac{I_{\text{CL}} + I_R}{C_{\text{DC}}}, 0, \frac{A_a C R_a k_l}{C_{\text{DC}} T_d} \left(\frac{V_G}{R_d} - I_{\text{CL}} - I_R \right) \\ & - \frac{A_a V_{M\_\text{ref}} k_l}{T_d}, 0, 0, \frac{A_b C R_b k_l}{C_{\text{DC}} T_d} \left(\frac{V_G}{R_d} - I_{\text{CL}} - I_R \right) \\ & - \frac{A_b V_{M\_\text{ref}} k_l}{T_d}, 0, 0, \frac{A_c C R_c k_l}{C_{\text{DC}} T_d} \left(\frac{V_G}{R_d} - I_{\text{CL}} - I_R \right) \\ & - \frac{A_c V_{M\_\text{ref}} k_l}{T_d}, 0 \Bigg]^T . \end{aligned} \tag{35}$$

In (34)

$$\gamma = -\frac{1}{C_{\text{DC}}} \left(\frac{1}{R_{\text{CL}}} + \frac{1}{R_R} + \frac{1}{R_d} + \sum_{x=\{a,b,c\}} \frac{1}{R_x} \right) \tag{36}$$

$$\forall x = \{a, b, c\}, \begin{cases} \alpha_x = \dfrac{A_x k_l C R_x}{C_{\text{DC}} T_d} \left(\dfrac{C_{\text{DC}}}{C R_x} + \dfrac{C_{\text{DC}}}{C R_x k_l} - \dfrac{1}{R_{\text{CL}}} \right. \\ \qquad \left. - \dfrac{1}{R_R} - \dfrac{1}{R_d} - \sum_{x=\{a,b,c\}} \dfrac{1}{R_x} \right) \\ \beta_x = \dfrac{A_x C R_x k_l}{C_{\text{DC}} T_d} \sum_{x=\{a,b,c\}} \dfrac{1}{R_x}. \end{cases} \tag{37}$$

For voltage boosting operation, e.g., when $0 < V_e < V_{T\_b}$, (38) shown at the bottom of the next page, and

$$\begin{aligned} C = \Bigg[& \frac{V_G}{R_d C_{\text{DC}}} - \frac{I_{\text{CL}} + I_R}{C_{\text{DC}}}, 0, \frac{A_a C R_a k_a}{C_{\text{DC}} T_d} \left(\frac{V_G}{R_d} - I_{\text{CL}} - I_R \right) \\ & - \frac{A_a V_{M\_\text{ref}} k_a}{T_d}, 0, 0, - \frac{A_b V_{\text{ref\_}b}}{T_d}, 0, 0, - \frac{A_c V_{\text{ref\_}c}}{T_d}, 0 \Bigg]^T . \end{aligned} \tag{39}$$

In (38)

$$\forall x = \{a, b, c\}, \begin{cases} \alpha'_x = \dfrac{A_x k_x C R_x}{C_{\text{DC}} T_d} \left(\dfrac{C_{\text{DC}}}{C R_x} + \dfrac{C_{\text{DC}}}{C R_x k_x} - \dfrac{1}{R_{\text{CL}}} \right. \\ \qquad \left. - \dfrac{1}{R_R} - \dfrac{1}{R_d} - \sum_{x=\{a,b,c\}} \dfrac{1}{R_x} \right) \\ \beta'_x = \dfrac{A_x C R_x k_x}{C_{\text{DC}} T_d} \sum_{x=\{a,b,c\}} \dfrac{1}{R_x}. \end{cases} \tag{40}$$

Since the other voltage boosting operating conditions are similar to the case of (38) and (39), the corresponding formulas are not provided here. The steady-state operating point X_S of the dc MG can be derived by solving

$$\begin{aligned} A \cdot X_S + C &= 0 \\ X_S &= -A^{-1} C. \end{aligned} \tag{41}$$

By substituting the solutions of (41) into (34) and (38), the small-signal stability of the series ES integrated dc MG at the steady-state operating point can be analyzed.

B. Case Study

1) Voltage Suppression Operation: When the RG reaches its maximum power generation ($P_R = 2216$ W), the dc MG is overvoltage and all series ESs will be operated in droop

$$A = \begin{bmatrix} \gamma & \frac{1}{C_{\text{DC}} R_a} & 0 & 0 & \frac{1}{C_{\text{DC}} R_b} & 0 & 0 & \frac{1}{C_{\text{DC}} R_c} & 0 & 0 \\ \frac{1}{C R_a} & -\frac{1}{C R_a} & 0 & -\frac{1}{C} & 0 & 0 & 0 & 0 & 0 & 0 \\ \alpha_a & \beta_a & -\frac{1}{T_d} & -\frac{A_a R_a}{T_d} & 0 & 0 & 0 & 0 & 0 & 0 \\ 0 & 0 & 0.2\pi f_s & -0.2\pi f_s & 0 & 0 & 0 & 0 & 0 & 0 \\ \frac{1}{C R_b} & 0 & 0 & 0 & -\frac{1}{C R_b} & 0 & -\frac{1}{C} & 0 & 0 & 0 \\ \alpha_b & 0 & 0 & 0 & \beta_b & -\frac{1}{T_d} & -\frac{A_b R_b}{T_d} & 0 & 0 & 0 \\ 0 & 0 & 0 & 0 & 0 & 0.2\pi f_s & -0.2\pi f_s & 0 & 0 & 0 \\ \frac{1}{C R_c} & 0 & 0 & 0 & 0 & 0 & 0 & -\frac{1}{C R_c} & 0 & -\frac{1}{C} \\ \alpha_c & 0 & 0 & 0 & 0 & 0 & 0 & \beta_c & -\frac{1}{T_d} & -\frac{A_c R_c}{T_d} \\ 0 & 0 & 0 & 0 & 0 & 0 & 0 & 0 & 0.2\pi f_s & -0.2\pi f_s \end{bmatrix} \tag{34}$$

mode. By gradually changing k_l from 0.1 to 7.85, calculating the corresponding X_S and A, the poles of the linearized dc MG can be plotted as shown in Fig. 9(a). When k_l increases, the poles on the left-hand side are moving rightward and the dominant poles are moving leftward. The increase of k_l will render that the left-side poles move toward the right half-plane, which results instability [37]. For a conservative design, k_l is set to be 7.85. Since all poles are located on the left half-plane, the system is stable.

2) Voltage Boosting Operation: When $P_R = -600$ W, ES_a will be operated in droop mode to boost the PCC voltage. Meanwhile, V_b and V_c are controlled to be 0 V. Similarly, the poles of the linearized dc MG can be plotted with respect to k_a as shown in Fig. 9(b). When k_a is gradually changed from 0.1 to 30, the dominant poles on the right-hand side are moving toward the left-hand side. While the poles on the left-hand side are moving rightward. Here, k_a is designed to be 30 to avoid the right-half-plane poles. As illustrated in Fig. 9(b), all poles of the system are on the left half-plane and the system is stable.

By following the same procedure, the system poles of the linearized dc MG with $P_R = 450$ W and $P_R = 0$ W can be plotted as shown in Fig. 9(c) and (d). By setting $k_b = 15$ and $k_c = 10$, the system stability can be guaranteed. Consequently, the voltage thresholds can be calculated as

$$\begin{cases} V_{\text{LB}} = \dfrac{V_{\min}}{k_l} = -7.6 \text{ V} \\ V_{T\_a} = 0 \text{ V} \\ V_{T\_b} = V_{T\_a} + \dfrac{V_{\max}}{k_a} = 2 \text{ V} \\ V_{T\_c} = V_{T\_b} + \dfrac{V_{\max}}{k_b} = 6 \text{ V} \\ V_{\text{UB}} = V_{T\_c} + \dfrac{V_{\max}}{k_c} = 12 \text{ V}. \end{cases} \tag{42}$$

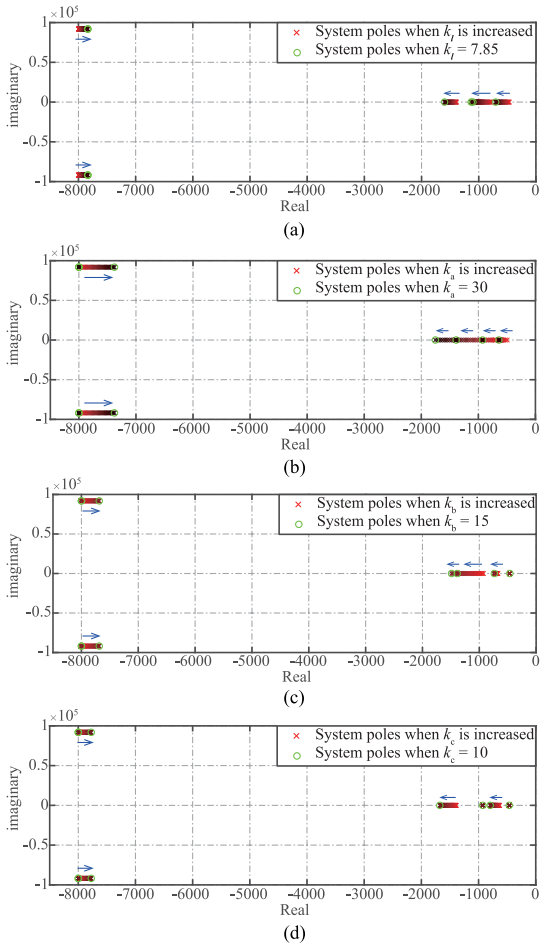

Fig. 9. Poles of the linearized dc MG when droop coefficients are gradually changed. (a) $P_R = -2216$ W, ES_a, ES_b, and ES_c are operated in droop mode. (b) $P_R = -600$ W, $V_b = V_c = 0$ V, and ES_a is operated in droop mode. (c) $P_R = -450$ W, $V_a = V_{\max}$, $V_c = 0$ V, and ES_b is operated in droop mode. (d) $P_R = 0$ W, $V_a = V_b = V_{\max}$, and ES_c is operated in droop mode.

$$A = \begin{bmatrix} \gamma & \dfrac{1}{C_{\text{DC}}R_a} & 0 & 0 & \dfrac{1}{C_{\text{DC}}R_b} & 0 & 0 & \dfrac{1}{C_{\text{DC}}R_c} & 0 & 0 \\ \dfrac{1}{CR_a} & -\dfrac{1}{CR_a} & 0 & -\dfrac{1}{C} & 0 & 0 & 0 & 0 & 0 & 0 \\ \alpha_a' & \beta_a' & -\dfrac{1}{T_d} & -\dfrac{A_aR_a}{T_d} & 0 & 0 & 0 & 0 & 0 & 0 \\ 0 & 0 & 0.2\pi f_s & -0.2\pi f_s & 0 & 0 & 0 & 0 & 0 & 0 \\ \dfrac{1}{CR_b} & 0 & 0 & 0 & -\dfrac{1}{CR_b} & 0 & -\dfrac{1}{C} & 0 & 0 & 0 \\ \dfrac{A_b}{T_d} & 0 & 0 & 0 & 0 & -\dfrac{1}{T_d} & -\dfrac{A_bR_b}{T_d} & 0 & 0 & 0 \\ 0 & 0 & 0 & 0 & 0 & 0.2\pi f_s & -0.2\pi f_s & 0 & 0 & 0 \\ \dfrac{1}{CR_c} & 0 & 0 & 0 & 0 & 0 & 0 & -\dfrac{1}{CR_c} & 0 & -\dfrac{1}{C} \\ \dfrac{A_c}{T_d} & 0 & 0 & 0 & 0 & 0 & 0 & 0 & -\dfrac{1}{T_d} & -\dfrac{A_cR_c}{T_d} \\ 0 & 0 & 0 & 0 & 0 & 0 & 0 & 0 & 0.2\pi f_s & -0.2\pi f_s \end{bmatrix} \tag{38}$$

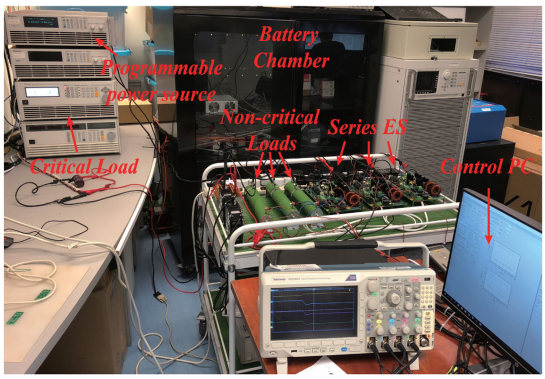

Fig. 10. Experimental setup of the series ES integrated dc MG.

VII. Experiment and Simulation Results

Experiments on a 120-V dc MG have been conducted to verify the storage reduction functionality of the proposed control strategy. The circuit diagrams of the dc MG and the series ES are shown in Figs. 1(b) and 4, respectively. The hardware implementation of the experiment setup is shown in Fig. 10. The corresponding specifications are listed in Table I. The intermittent RG and the main dc source are emulated by a programmable dc power supply (Chroma 60150H 600S). It is controlled to inject a fluctuating power to the system. The CL is emulated by a dc electronic load (Chroma 63802). It draws a constant dc power of 400 W from the grid. ES_a, ES_b, and ES_c are connected in series with a light load (144 Ω), a medium load (72 Ω), and a heavy load (48 Ω), respectively. There are five pieces of valve-regulated-lead-acid batteries installed as the dc-link storage of each series ES. Each battery has a terminal voltage of 12 V. Considering the acceptable voltage and power variation of typical NCLs, such as water heater [38], [39] and water electrolyser [40], the ES output voltages are limited between −60 V and +60 V for experimental demonstrations. The decentralized voltage controllers are programmed in the digital signal processors (TMS320F28069) to control the series ESs.

A. Charging and Discharging Power Curves of Batteries

In this experiment, the power of the programmable dc power supply is changed from 692 to 1548 W so that P_{OS} will be varied from −419 to 437 W. For the first set of experiments, the series ESs are controlled by the proposed droop controller to regulate V_M to be within the vicinity of 120 V. For the second set of experiments, the series ESs are controlled by a conventional droop controller to restore V_M to the same voltage level. This conventional droop controller will operate all series ESs to have nearly identical charging and discharging power until the series ESs reach the output voltage limits. The experiment results are shown in Fig. 11.

Fig. 11(a) shows the total battery power P_T with respect to the variation of P_{OS}. By subtracting P_T of the conventional controller from that of the proposed controller, the power difference between the two curves shown in Fig. 11(a) can be plotted as shown in Fig. 11(b). In the voltage boosting operation,

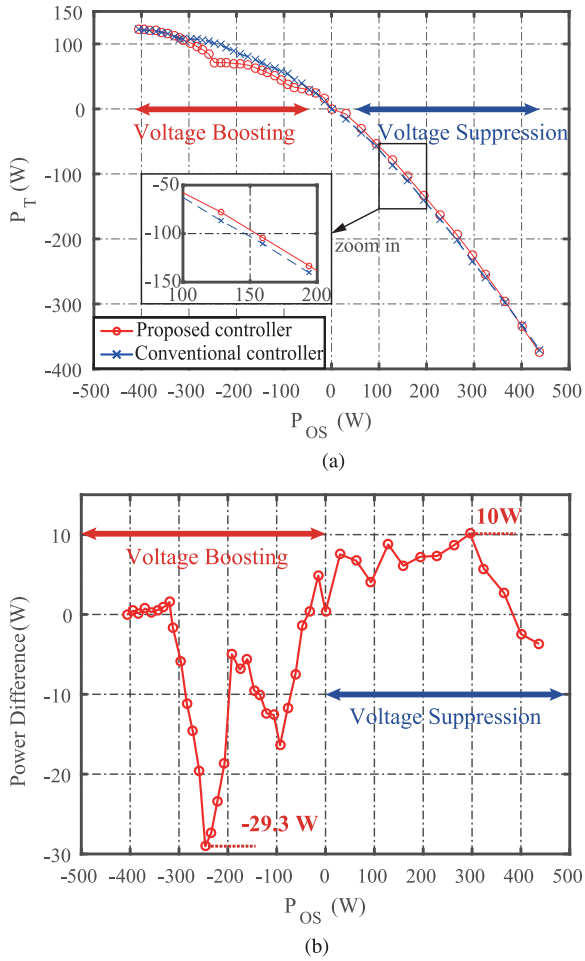

Fig. 11. (a) Measured P_T and (b) power difference with respect to the change of P_{OS}. (a) Measured P_T with respect to the change of P_{OS}. (b) Power difference with respect to the change of P_{OS}.

the charging power of batteries with the proposed controller is smaller than that of the conventional controller. The maximum reduced charging power is as large as 29.3 W. This means that the proposed controller can effectively reduce the charging power of the batteries and thus the battery capacity can be reduced. In the voltage suppression operation, the discharging power of batteries with the proposed controller is smaller than that of the conventional controller. The maximum reduced discharging power is as large as 10 W. This means that the proposed controller can decrease the discharging power of the batteries and that the storage capacity required for delivering energy can be reduced. When P_{OS} approaches 400 or −400 W, the power difference will become nearly 0 W since the series ES voltages will reach the output limits.

B. Stabilizing DC Bus Voltage

In this experiment, the programmable dc source is controlled to generate a randomly fluctuating power to the system for 200 s. The time profile of the generated power is shown in Fig. 12. The series ESs will be controlled to regulate V_M to be within

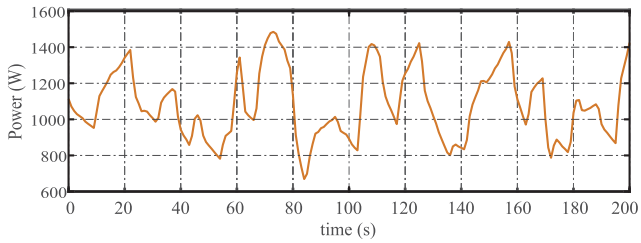

Fig. 12. Time profile of the generated power of the programmable source.

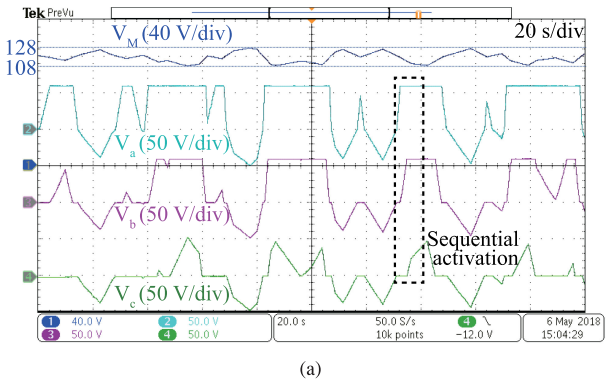

(a)

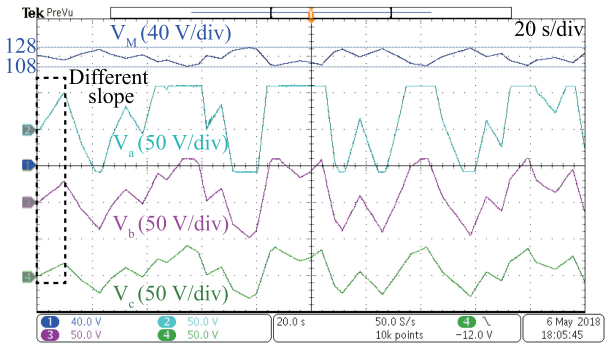

(b)

Fig. 13. Experiment waveforms of bus voltage and series ES voltages with (a) proposed controller and (b) conventional controller.

the vicinity of 120 V by using the proposed controller and the conventional controller.

Fig. 13 shows the experimental waveforms of V_M and the series ES voltages under the two controllers. Both the proposed controller and the conventional controller will operate the series ESs to regulate V_M between 108 and 128 V. As shown in Fig. 13(a), when $V_M < 120$ V, the proposed controller will engage the series ESs in voltage boosting operation sequentially. When V_M decreases, V_a rises first to shed the light load until it reaches the maximum output voltage of 60 V. As V_M keeps decreasing, V_b starts to rise and the medium load is shed. When V_b reaches 60 V and V_M is falling, V_c increases to shed the heavy load. When $V_M > 120$ V, the proposed controller operates the series ESs at identical voltage levels to boost the NCLs.

As shown in Fig. 13(b), the conventional controller engages all series ESs in voltage boosting and suppression operations. However, the slopes of the ES voltage profiles are different. V_a with the light load has a steep slope and V_c with the heavy load

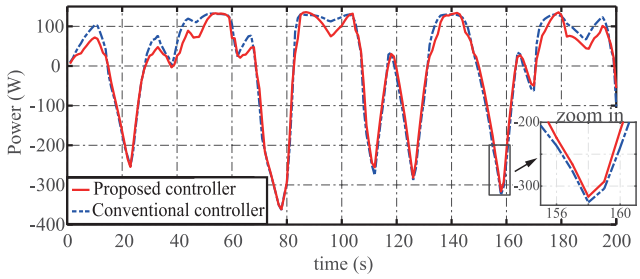

(a)

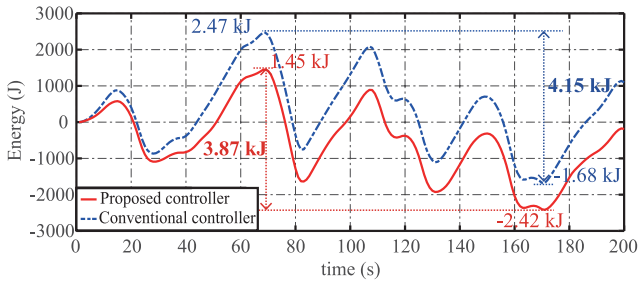

(b)

Fig. 14. Experiment waveforms of (a) total battery power and (b) total accumulated battery energy.

has a gentle slope. In this way, the powers of different series ESs can be controlled to be nearly identical.

The measured time profiles of the total battery power and total accumulated battery energy are plotted as shown in Fig. 14(a) and (b), respectively. As illustrated in Fig. 14(a), the charging and discharging power of the series ESs with the conventional controller is always larger than that of the proposed controller. This proves that the proposed controller can operate the series ESs to use a small amount of power to regulate V_M.

As shown in Fig. 14(b), for the conventional controller, the maximum stored and delivered energy of the series ESs' battery are 2.47 and -1.68 kJ, respectively. Thus, the maximum energy deviation of battery storages can be calculated as 4.15 kJ according to (10). For the proposed controller, the maximum stored and delivered energies are 1.45 and -2.42 kJ, respectively. The corresponding maximum energy deviation of battery storage can be calculated as 3.87 kJ, which is 92.5% of that of the conventional controller. Since the storage capacity should be sufficiently large to buffer the maximum possible energy deviation, the minimum required storage capacity of the series ES can be reduced by 7.5% by using the proposed controller. This proves that the proposed controller can effectively reduce the required storage capacity of the series ESs.

C. Dynamic Response

In this experiment, the output voltage of the programmable power supply is controlled to step up from 134.2 to 142 V. The three sets of series ESs are operated by the proposed controller to suppress the bus voltage.

The experiment waveforms are shown in Fig. 15. When the bus voltage V_M surges, the three series ESs output negative dc voltage of -33 V to boost the NCLs. With the support of the

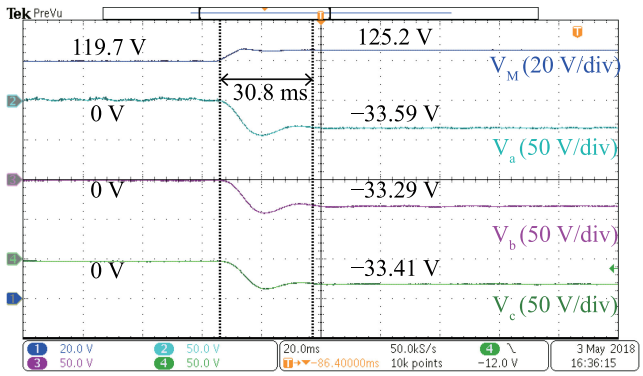

Fig. 15. Experiment waveforms of transient responses of multiple series ESs.

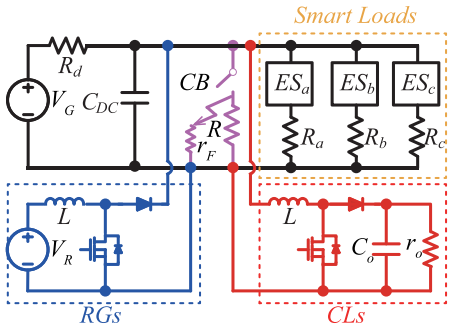

Fig. 16. Circuit schematic diagram of the simulated faulted dc MG.

series ESs, the bus voltage is stabilized at 125.2 V in 30.8 ms. As illustrated in Fig. 15, the voltage waveforms of the three ESs fluctuated for around one cycle before settling at an identical value. The controller can ensure that the dynamic responses of the series ESs are almost identical. This assures that the voltages of the series ESs are always the same such that the minimum discharging power of the series ESs can be obtained.

D. Voltage Responses During Grid Fault

In order to demonstrate that the series ESs can assist the CPL to survive the fault, a simulation study of a faulted 14-kW dc MG is performed. The circuit schematic diagram of the simulated system is illustrated in Fig. 16 and the corresponding specifications are listed in Table III. The RG is simulated by a boost converter, which converts a dc power of 4.1 kW from a 60-V dc source V_R to the grid. Whereas the main dc source is delivering 6.5 kW to the grid. The CPL is essentially a boost-converter-interfaced load with an output resistance of 20 Ω. It consistently absorbs a power of 4 kW from the grid. When the fault happens, a 4-kW resistive load R will be short circuited to a low resistance of 1 Ω. In the meantime, the series ESs will respond to hold the PCC voltage. After 10 ms, the faulted load R will be tripped from the MG to clear the fault. The simulated waveforms of the dc MG are shown in Fig. 17.

As shown in Fig. 17(a) and (b), before the fault occurs, V_M is stabilized at 120 V and the output voltage V_o of the CPL is regulated to 283 V. When the dc bus is short circuited at 0.02 s,

TABLE III
SPECIFICATIONS OF THE SIMULATION

Description	Parameter	Value
Main dc source	V_G	145 V
Distribution resistance	R_d	0.3 Ω
DC-link capacitance	C_{DC}	1000 μF
RG	P_R	4100 W
Filtering inductor	L	1 mH
Power reference of CPL	P_{CL}	4 kW
Filtering capacitor of CPL	C_o	100 μF
Output resistor of CPL	r_o	20 Ω
Switching frequency		100 kHz
NCL	R_a	14.4 Ω
	R_b	7.2 Ω
	R_c	4.8 Ω
Faulted load	R	3.6 Ω
Short-circuit resistor	r_F	1 Ω

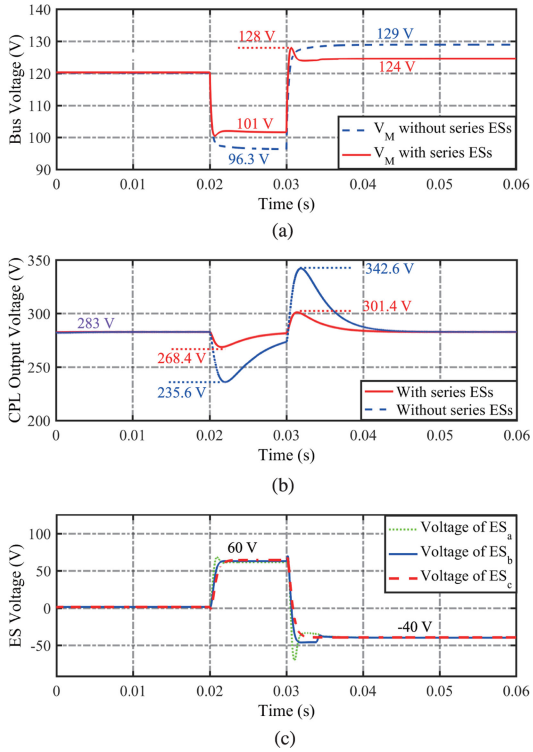

Fig. 17. Simulated voltage waveforms of CPL-integrated dc MGs with and without the series ESs. (a) DC bus voltages. (b) Output voltages of CPLs. (c) ES output voltages.

without the series ESs, V_M drops to 96.3 V and a voltage dip of 47.4 V is generated on V_o. Thereafter, the inherent control loop of CPL operates the boost converter to correct the voltage dip. At 0.03 s, R is tripped by the circuit breaker CB. Without the series ESs, V_M rises up to 129 V. Meanwhile, a voltage spike of 59.6 V is generated on the profile of V_o due to the surge of V_M.

When the series ESs activated, all series ESs are controlled to output a voltage of 60 V during the fault as shown in Fig. 17(c). Since the NCLs are shed by the series ESs, the voltage dip of V_M is alleviated. V_M drops to 101 V, which is higher than that in the case without the series ESs. After the fault is cleared, V_M surges to 128 V. Since then, the voltages of the series ESs are unanimously controlled at −40 V to suppress V_M at 124 V.

As illustrated in Fig. 17(b), the maximum voltage dip (14.6 V) and voltage spikes (18.4) of V_o with the series ESs are generally smaller than those in the case without the series ESs. This proves that the series ESs can quickly respond to the grid fault for reducing the impacts of bus voltage deviations on the CPL. Consequently, the CPL can better survive the fault.

VIII. Conclusion

The different power-rated NCLs will affect the charging and discharging power of the series ESs' battery storages. This offers the possibility of reducing the series ES storage capacity. The operating conditions of multiple series ESs in achieving the minimum charging and discharging power have been explicitly derived. Based on this, a decentralized controller that can reduce the total storage capacity of the series ESs has been designed and verified for a 120-V dc MG system. It is demonstrated that the series ESs can improve the voltage stability of a dc MG with a CPL. The experiment results have proved that the proposed decentralized controller can effectively coordinate the operations of multiple series ESs to reduce the total battery storage capacity in dc MGs.

Acknowledgment

The authors would like to thank Dr. Y. Jia and Y. He for their kind suggestions.

References

[1] K. Garbesi, V. Vossos, A. H. Sanstad, and G. Burch, "Optimizing energy savings from direct-DC in U.S. residential buildings," Lawrence Berkeley Nat. Lab., Berkeley, CA, USA, Tech. Rep. LBNL-5193E, Oct. 2011.

[2] *IEEE Recommended Practice for Utility Interface of Photovoltaic (PV) Systems*, IEEE Std 929-2000, 2000.

[3] Y. Jia *et al.*, "Powering China's sustainable development with renewable energies: Current status and future trend," *Elect. Power Compon. Syst.*, vol. 43, no. 8–10, pp. 1193–1204, 2015.

[4] C. S. Lai, Y. Jia, L. L. Lai, Z. Xu, M. D. McCulloch, and K. P. Wong, "A comprehensive review on large-scale photovoltaic system with applications of electrical energy storage," *Renewable Sustain. Energ Rev.*, vol. 78, pp. 439–451, 2017.

[5] M. Wang, T. Yang, S. Tan, and S. Y. Hui, "Hybrid electric springs for grid-tied power control and storage reduction in ac microgrids," *IEEE Trans. Power Electron.*, vol. 34, no. 4, pp. 3214–3225, Apr. 2019.

[6] Y. Zheng, D. J. Hill, K. Meng, and S. Y. Hui, "Critical bus voltage support in distribution systems with electric springs and responsibility sharing," *IEEE Trans. Power Syst.*, vol. 32, no. 5, pp. 3584–3593, Sep. 2017.

[7] H. D. Tafti, A. I. Maswood, G. Konstantinou, J. Pou, and F. Blaabjerg, "A general constant power generation algorithm for photovoltaic systems," *IEEE Trans. Power Electron.*, vol. 33, no. 5, pp. 4088–4101, May 2018.

[8] S. Kawachi *et al.*, "Energy capacity reduction of energy storage system in microgrid by use of heat pump: Characteristic study by use of actual machine," in *Proc. Int. Power Electron. Motion Control Conf.*, Sep. 2010, pp. T11-52–T11-58.

[9] Q. Wang, D. Zha, F. Deng, M. Cheng, and G. Buja, "A topology of DC electric springs for DC household applications," *IET Power Electron.*, vol. 12, no. 5, pp. 1241–1248, 2019.

[10] M. Wang, S. Yan, S. Tan, and S. Y. Hui, "Hybrid-DC electric springs for DC voltage regulation and harmonic cancellation in DC microgrids," *IEEE Trans. Power Electron.*, vol. 33, no. 2, pp. 1167–1177, Feb. 2018.

[11] L. Liang, Y. Hou, and D. J. Hill, "An interconnected microgrids based transactive energy system with multiple electric springs," *IEEE Trans. Smart Grid*, to be published, doi: 10.1109/TSG.2019.2919758.

[12] K. T. Mok, M. H. Wang, S. C. Tan, and S. Y. Hui, "DC electric springs—A new technology for stabilizing DC power distribution systems," *IEEE Trans. Power Electron.*, vol. 32, no. 2, pp. 1088–1105, Feb. 2017.

[13] M. H. Wang, K. T. Mok, S. C. Tan, and S. Y. Hui, "Multifunctional DC electric springs for improving voltage quality of DC grids," *IEEE Trans. Smart Grid*, vol. 9, no. 3, pp. 2248–2258, May 2018.

[14] M. Wang, S. Tan, C. Lee, and S. Y. Hui, "A configuration of storage system for DC microgrids," *IEEE Trans. Power Electron.*, vol. 33, no. 5, pp. 3722–3733, May 2018.

[15] C. Gavriluta, I. Candela, A. Luna, A. Gomez-Exposito, and P. Rodriguez, "Hierarchical control of HV-MTDC systems with droop-based primary and OPF-based secondary," *IEEE Trans. Smart Grid*, vol. 6, no. 3, pp. 1502–1510, May 2015.

[16] S. Moon, S. G. Yoon, and J. H. Park, "A new low-cost centralized MPPT controller system for multiply distributed photovoltaic power conditioning modules," *IEEE Trans. Smart Grid*, vol. 6, no. 6, pp. 2649–2658, Nov. 2015.

[17] J. Schonbergerschonberger, R. Duke, and S. D. Round, "DC-bus signaling: A distributed control strategy for a hybrid renewable nanogrid," *IEEE Trans. Ind. Electron.*, vol. 53, no. 5, pp. 1453–1460, Oct. 2006.

[18] X. Chen, M. Shi, H. Sun, Y. Li, and H. He, "Distributed cooperative control and stability analysis of multiple DC electric springs in DC microgrid," *IEEE Trans. Ind. Electron.*, vol. 65, no. 7, pp. 5611–5622, Jul. 2018.

[19] Y. Zheng, C. Zhang, D. J. Hill, and K. Meng, "Consensus control of electric spring using back-to-back converter for voltage regulation with ultra-high renewable penetration," *J. Mod. Power Syst. Clean Energy*, vol. 5, no. 6, pp. 897–907, Nov. 2017.

[20] X. Chen, Y. Hou, and S. Y. Hui, "Distributed control of multiple electric springs for voltage control in microgrid," *IEEE Trans. Smart Grid*, vol. 8, no. 3, pp. 1350–1359, May 2017.

[21] Y. R. Mohamed and E. F. El-Saadany, "Adaptive decentralized droop controller to preserve power sharing stability of paralleled inverters in distributed generation microgrids," *IEEE Trans. Power Electron.*, vol. 23, no. 6, pp. 2806–2816, Nov. 2008.

[22] A. Khorsandi, M. Ashourloo, and H. Mokhtari, "A decentralized control method for a low-voltage DC microgrid," *IEEE Trans. Energy Convers.*, vol. 29, no. 4, pp. 793–801, Dec. 2014.

[23] X. Lu, K. Sun, J. M. Guerrero, J. C. Vasquez, and L. Huang, "Double-quadrant state-of-charge-based droop control method for distributed energy storage systems in autonomous DC microgrids," *IEEE Trans. Smart Grid*, vol. 6, no. 1, pp. 147–157, Jan. 2015.

[24] J. Li, Z. Xu, J. Zhao, S. Chai, Y. Yu, and X. Xu, "Model predictive control based ramp minimization in active distribution network using energy storage systems," *Elect. Power Compon. Syst.*, vol. 47, no. 3, pp. 201–211, 2019.

[25] M. L. N. Chen, L. J. Jiang, and W. E. I. Sha, "Ultrathin complementary metasurface for orbital angular momentum generation at microwave frequencies," *IEEE Trans. Antennas Propag.*, vol. 65, no. 1, pp. 396–400, Jan. 2017.

[26] J. Li, Z. Xu, J. Zhao, and C. Zhang, "Distributed online voltage control in active distribution networks considering PV curtailment," *IEEE Trans. Ind. Inform.*, to be published, doi: 10.1109/TII.2019.2903888.

[27] Y. Gu, X. Xiang, W. Li, and X. He, "Mode-adaptive decentralized control for renewable DC microgrid with enhanced reliability and flexibility," *IEEE Trans. Power Electron.*, vol. 29, no. 9, pp. 5072–5080, Sep. 2014.

[28] X. Lu, K. Sun, J. M. Guerrero, J. C. Vasquez, and L. Huang, "State-of-charge balance using adaptive droop control for distributed energy storage systems in DC microgrid applications," *IEEE Trans. Ind. Electron.*, vol. 61, no. 6, pp. 2804–2815, Jun. 2014.

[29] X. Lu, J. M. Guerrero, K. Sun, and J. C. Vasquez, "An improved droop control method for DC microgrids based on low bandwidth communication with DC bus voltage restoration and enhanced current sharing accuracy," *IEEE Trans. Power Electron.*, vol. 29, no. 4, pp. 1800–1812, Apr. 2014.

[30] Q. Xu, J. Xiao, P. Wang, and C. Wen, "A decentralized control strategy for economic operation of autonomous AC, DC, and hybrid AC/DC microgrids," *IEEE Trans. Energy Convers.*, vol. 32, no. 4, pp. 1345–1355, Dec. 2017.

[31] S. Y. Hui, C. K. Lee, and F. F. Wu, "Electric springs-a new smart grid technology," *IEEE Trans. Smart Grid*, vol. 3, no. 3, pp. 1552–1561, Sep. 2012.

[32] G. Chu, C. K. Tse, S. C. Wong, and S. C. Tan, "A unified approach for the derivation of robust control for boost PFC converters," *IEEE Trans. Power Electron.*, vol. 24, no. 11, pp. 2531–2544, Nov. 2009.

[33] A. Kelly and K. Rinne, "Control of DC-DC converters by direct pole placement and adaptive feedforward gain adjustment," in *Proc. IEEE Appl. Power Electron. Conf. Expo.*, Mar. 2005, vol. 3, pp. 1970–1975.

[34] Y. Xia, W. Wei, M. Yu, and P. Wang, "Stability analysis of PV generators with consideration of P&O-based power control," *IEEE Trans. Ind. Electron.*, vol. 66, no. 8, pp. 6483–6492, Aug. 2019.

[35] A. M. Rahimi and A. Emadi, "Active damping in DC/DC power electronic converters: A novel method to overcome the problems of constant power loads," *IEEE Trans. Ind. Electron.*, vol. 56, no. 5, pp. 1428–1439, May 2009.
[36] Q. Shafiee, T. Dragiĉević, J. C. Vasquez, and J. M. Guerrero, "Hierarchical control for multiple DC-microgrids clusters," *IEEE Trans. Energy Convers.*, vol. 29, no. 4, pp. 922–933, Dec. 2014.
[37] J. M. Guerrero, M. Chandorkar, T. Lee, and P. C. Loh, "Advanced control architectures for intelligent microgrids—Part I: Decentralized and hierarchical control," *IEEE Trans. Ind. Electron.*, vol. 60, no. 4, pp. 1254–1262, Apr. 2013.
[38] L. Liang, Y. Hou, and D. J. Hill, "Enhancing flexibility of an islanded microgrid with electric springs," *IEEE Trans. Smart Grid*, vol. 10, no. 1, pp. 899–909, Jan. 2019.
[39] *Household and Similar Electrical Appliances—Safety—Part 2-45: Particular Requirements for Portable Heating Tools and Similar Appliances*," IEC 60335-2-45:2002, Oct. 2002.
[40] M. Carmo, D. L. Fritz, J. Mergel, and D. Stolten, "A comprehensive review on PEM water electrolysis," *Int. J. Hydrogen Energy*, vol. 38, no. 12, pp. 4901–4934, 2013.

Ming-Hao Wang (S'15–M'18) received the B.Eng. (Hons.) degree in electrical and electronic engineering from the Huazhong University of Science and Technology, Wuhan, China, and the University of Birmingham, Birmingham, U.K., in 2012, and M.Sc. and Ph.D. degrees in electrical and electronic engineering from The University of Hong Kong, Hong Kong, in 2013 and 2017, respectively.

He is currently a Postdoctoral Research Fellow with the Department of Electrical Engineering, The Hong Kong Polytechnic University, Hong Kong. His research interests include dc power systems and power electronics.

Shuo Yan (S'13–M'16) received the B.Eng. degree in electrical engineering from the University of South China, Hengyang, China, in 2007, the M.Eng. degree in electrical engineering from Southeast University, Nanjing, China, in 2010, and Ph.D. degree in electrical engineering from The University of Hong Kong, Hong Kong, in 2016.

He was a Postdoctoral Fellow in power electronics and control with The University of Hong Kong from 2016 to 2019. He is currently a Senior Lecturer with RMIT University, Melbourne VIC, Australia. His current research interests include power electronics, smart grids, and renewable energy.

Siew-Chong Tan (M'06–SM'11) received the B.Eng. (Hons.) and M.Eng. degrees in electrical and computer engineering from the National University of Singapore, Singapore, in 2000 and 2002, respectively, and the Ph.D. degree in electronic and information engineering from The Hong Kong Polytechnic University, Hong Kong, in 2005.

From October 2005 to May 2012, he was a Research Associate, a Postdoctoral Fellow, a Lecturer, and an Assistant Professor with the Department of Electronic and Information Engineering, The Hong Kong Polytechnic University. From January to October 2011, he was a Senior Scientist with Agency for Science, Technology, and Research (A*Star), Singapore. He is currently a Professor with the Department of Electrical and Electronic Engineering, The University of Hong Kong. He is a co-author of the book *Sliding Mode Control of Switching Power Converters: Techniques and Implementation* (CRC Press, 2011).

Dr. Tan is a Reviewer for various IEEE/IET transactions and journals on power, electronics, circuits, and control engineering. He is an Associate Editor for the IEEE TRANSACTIONS ON POWER ELECTRONICS.

Zhao Xu (M'2016–SM'2012) received the B.Eng. degree from Zhejiang University, Hangzhou, China, in 1996, the M.Eng. degree from the National University of Singapore, Singapore, in 2002, and Ph.D. degree from The University of Queensland, Brisbane, QLD, Australia, in 2006, all in electrical engineering.

From 2006 to 2009, he was an Assistant Professor and later an Associate Professor with the Centre for Electric Technology, Technical University of Denmark, Kongens Lyngby, Denmark. Since 2010, he has been with The Hong Kong Polytechnic University, Hong Kong, where he is currently a Professor with the Department of Electrical Engineering and a Leader of Smart Grid Research Area. He is also in the foreign Associate Staff of the Centre for Electric Technology, Technical University of Denmark. His research interests include demand side, grid integration of wind and solar power, electricity market planning and management, and artificial intelligence applications.

Dr. Xu is an Editor for the Electric Power Components and Systems, the IEEE PES Power Engineering Letter, and the IEEE TRANSACTIONS ON SMART GRID. He is currently the Chairman of IEEE PES/IES/PELS/IAS Joint Chapter in Hong Kong Section.

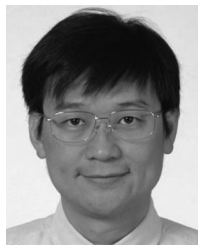

Shu Yuen (Ron) Hui (M'87–SM'94–F'03) received the B.Sc.Eng. (Hons.) degree in electrical and electronic engineering from the University of Birmingham, Birmingham, U.K., in 1984, and the D.I.C. and Ph.D. degrees from Imperial College London, London, U.K., in 1987.

Since July 2010, he has been a part-time Chair Professor of Power Electronics with Imperial College London and the Philip Wong Wilson Wong Professor with The University of Hong Kong, Hong Kong. He has authored or coauthored more than 220 refereed journal publications and book chapters, and more than 60 of his patents have been adopted by industry.

Dr. Hui is a Fellow of the Australian Academy of Technological Sciences and Engineering and the Royal Academy of Engineering (U.K.). He is an Associate Editor for the IEEE TRANSACTIONS ON POWER ELECTRONICS and IEEE TRANSACTIONS ON INDUSTRIAL ELECTRONICS. He was the recipient of the 2010 IEEE Rudolf Chope R&D Award from the IEEE Industrial Electronics Society, the 2010 IET Crompton Medal, and the 2015 IEEE William E. Newell Power Electronics Award.